INVESTIGATIONS OF HALF-METALLICITY AMONG DOPED AND UN-DOPED GRAPHENE NANOSTRUCTURES IN DIFFERENT CONFORMATIONS FOR SPINTRONICS APPLICATIONS

BERHANU TELAY MEKONNEN

A THESIS SUBMITTED TO

THE MATERIALS SCIENCE PROGRAM

PRESENTED IN PARTIAL FULFILMENT OF THE REQUIREMENTS FOR THE DEGREE OF MASTER OF SCIENCE IN MATERIALS SCIENCE

ADDIS ABABA UNIVERSITY

ADDIS ABABA, ETHIOPIA

JUNE 2012

ADDIS ABABA UNIVERSITY

SCHOOL OF GRADUATE STUDIES

This is to certify that the thesis prepared by Berhanu Telay Mekonnen entitled: Investigations of Half-Metallicity among Doped and Un-doped Graphene Nanostructures for Spintronics Applications and submitted in partial fulfillment of the requirements for the degree of Degree of Master of Sciences (Materials Science) complies with the regulations of the University and meets the accepted standards with respect to originality and quality.

Signed by the Examining Committee:

Examiner: Dr. Gebre Medhen G/Yesus Signature _____ Date 27/06/2012

Examiner: Dr. Tilak Bollepalli Signature _____ Date 27/06/2012

Advisor: Prof. Javed Mazher Signature _____ Date 27/06/2012

Chairman: Prof. Teketel Yohannes Signature _____ Date 27/06/2012

Abstract

We have investigated the phenomenal of half-metallicity among various novel conformations of graphene nanoribbons (GNRs). The Density of States (DOS) and the Transmission spectrum (TS) of zigzag GNRs doped with boron (B), Nitrogen (N) and Oxygen (O) atoms and undoped but with vacancies are independently investigated by first-principle calculations. A new scheme of spin diode architecture is identified to achieve half-metallicity in ZGNRs by doping B atoms at one edge and N atoms at the other as well as B atom at one edge and O atom at the other edge. We found that the origin of the nearly half-metallic state is due to interactions between the edge states and B-N or B-O atoms which provide direct control over the electron occupation of the edge states by inducing large chemical potential difference between the edge states. We have also found that the ZGNR spintronicity is vacancy concentration dependent. Particularly, for single vacancy site the FM coupling among the zigzag edges are more favorable, while double vacancy sites are found to promote the AFM edge coupling. The as mentioned results of the nearly half-metallicity are presented in the thesis by corroborating them with the results of spin polarization. The prospects of nearly half metallic results are also discussed in context to mangetoresistive device performance.

Acknowledgement

I would like to thank the Addis Ababa University Graduate Studies Program for giving me the chance to join the Materials Science Masters program. And I would like to extend my acknowledgement to the Materials Science Program for providing me all the facilities required for this thesis. Finally, I would like to thank my advisor Prof. Javed Mazher for guiding me to complete this thesis.

Table of Contents

Contents **Pages**

List of Tables

List of Figures

CHAPTER ONE

1. Introduction

Graphene is an allotrope of carbon, whose structure is one-atom-thick planar sheets of sp^2-bonded carbon atoms that are densely packed in a honeycomb crystal lattice. Since its production in 2004, it has become the hottest research issue due to its outstanding electronic as well as mechanical properties.

Normally, the two-dimensional (2D) intrinsic graphene sheet is semimetallic or zero-gap semiconductor. However, when the 2D sheet is cut into rectangular slices, namely, the graphene nanoribbons (GNRs), they can become semiconductors with the band gap depending on the width of GNRs as well as the crystallographic orientation of cutting edges. Hence, GNRs possess tunable electronic properties, rendering GNR-based nanoelectronic devices possible [1]. Besides the width-dependent semiconducting properties, previous theoretical studies have also revealed that zigzag-edged GNRs (ZGNRs) can be converted into half metals by either applying an external electric filed or through chemical modification of the edges [2, 3]. Half metals hold the promise for spintronic applications as the electric current is fully spin polarized when going through half metals because one electron spin channel is insulating while the other is metallic.

In this thesis we have performed a theoretical investigation on zigzag graphene nanoribbons using the ab initio SIESTA code to determine a specific conformation of zigzag graphene nanoribbon with better half-metallic behavior.

1.1. Graphene

Graphene is the name given to a flat monolayer of carbon atoms tightly packed into a two-dimensional (2D) honeycomb lattice, and is a basic building block for graphitic materials of all other dimensionalities as depicted in figure 1.1. It can be wrapped up into 0D fullerenes, rolled into 1D nanotube or stacked into 3D graphite.

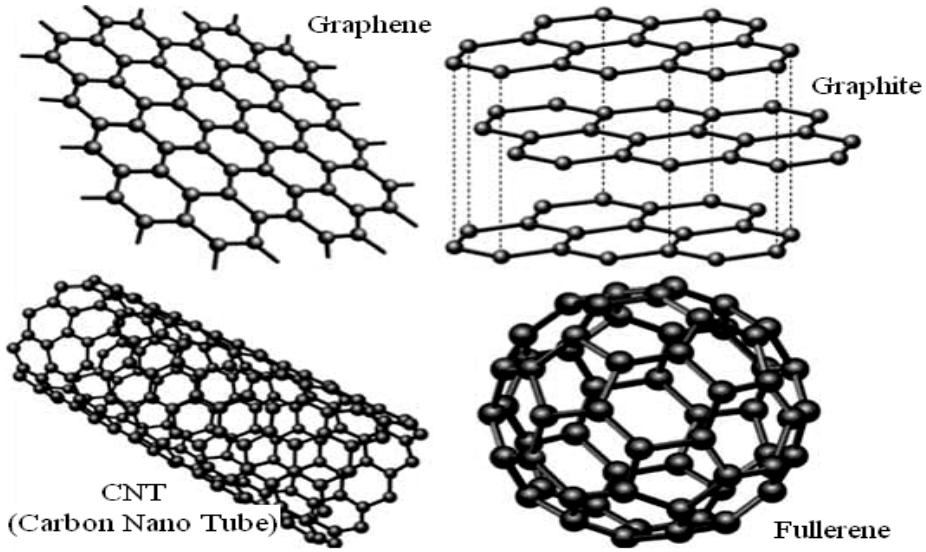

Figure 1.1 Schematic diagram of Graphene and its derivatives, Graphite, Fullernene and Carbon nano tube (CNT)[4].

1.1.1 Structure of Graphene

Graphene consists of a single layer of carbon atoms, arranged in a honeycomb lattice. It has been studied theoretically for a long time as a building block of graphitic materials in other dimensions. The most famous allotrope of graphene is graphite, consisting of stacked graphene layers, held together only by weak Van der Waals forces. One-dimensional carbon nanotubes and zero-dimensional fullerenes can be described as rolled

up graphene sheets. But in contrast to these materials, isolated graphene was expected to be thermodynamically unstable and therefore not to exist in real life until its discovery in 2004 [5].

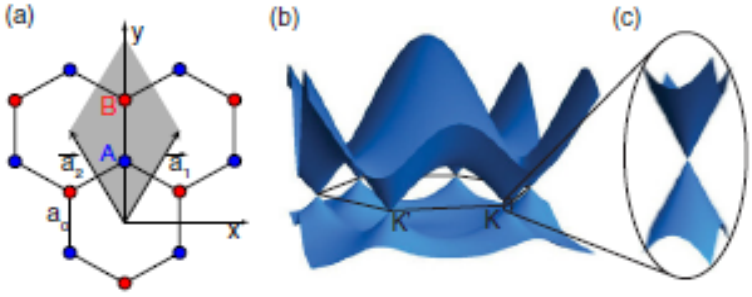

Figureure 1.2 (a) Lattice structure of graphene. The atoms belonging to the two sub-lattices A and B are represented by circles; the lines between the circles indicate the chemical bonds. a_0 is the nearest-neighbor distance. The unit cell is depicted in gray, together with the primitive lattice vectors a_1 and a_2. (b) Band structure of graphene. (c) Zoom of the dispersion relation close to the K-point for small energies [6].

The covalent bonds between nearest-neighbor carbon atoms in graphene are formed by sp^2-hybridized orbitals. These strong bonds give graphene its extraordinary mechanical strength, making it possible to have stable free-standing graphene sheets, being only one atomic layer thick. The remaining p-electron per atom is delocalized over the whole graphene lattice, and is responsible for the electric conductivity. Figure1.2 (a) represents the lattice structure of graphene. The graphene lattice consists of two interpenetrating sub-lattices, denoted by A and B depicted in blue (dark gray) and red (light gray). The unit cell, indicated in gray, therefore comprises two atoms, one of each sub-lattice. The nearest neighbor distance is a_0 = 1.42Å. In reciprocal space, the first Brillouin zone also

has a hexagonal shape as shown in figure 1.2(b) [6]. Valence and conduction bands touch at the K and K' points at the corners of the first Brillouin zone, with a linear dispersion for small enough energies, figure 1.2(c). Around the K and K' points the dispersion relation of graphene can be described by the expression $E_{\pm}(\vec{q}) \approx \pm \mathrm{h}\nu_F|\vec{q}|$, with $\nu_F \approx 1 \times 10^6$ m s^{-1}. In un-doped graphene, the Fermi energy lies exactly at the Dirac point which implies that the π-band is completely filled, while the π^* - band is empty.

This linear dispersion relation, together with the so-called pseudospin related to the two sublattices and the electron–hole symmetry, implies that the low-energy properties of graphene charge carriers can be described by the 2D massless Dirac equation: $-i\nu_F\vec{\sigma}.\nabla\psi(\vec{r}) = E\psi(\vec{r})$, where $\vec{\sigma} = (\sigma_x, \sigma_y)$ are the Pauli matrices. Although there is nothing relativistic about the electrons in graphene, the band structure resulting from the honeycomb lattice makes it possible to describe them like massless Dirac fermions, which gives rise to some of the unusual transport properties of graphene.

1.1.2 Electronic Properties of Graphene:

From the point of view of its electronic properties, graphene is a two dimensional zero-gap semiconductor and the low-energy charge carriers formally described by the Dirac-like Hamiltonian exhibit Fermi velocity of $\nu_F \approx 10^6$ m/s [7]. Neglecting many-body effects, this description is accurate theoretically and has also been proven experimentally by measuring the energy-dependent cyclotron mass in graphene (which yields its linear

energy spectrum) and, most clearly by the observation of a relativistic analogue of the integer quantum hall effect (QHE).

The fact that charge carriers in graphene are described by the Dirac-like equation rather than the usual Schroedinger equation can be seen as a consequence of graphene's crystal structure, which consists of two equivalent carbon sub-lattices A and B as shown in the figure 1.2(a). A quantum mechanical hopping between the sub-lattices leads to the formation of two energy bands, and their intersection near the edges of the Brillouin zone yields the conical energy spectrum near the "Dirac" points K and K' as shown in the figure 1.2(b) as a result, the quasiparticles in graphene exhibit the linear dispersion relation $E = \hbar k v_F$ as if they are massless relativistic particles, with the role of the speed of light played by the Fermi velocity $v_F \approx c/300$. Thus owing to the linear spectrum, one can expect that these quasiparticles behave differently from those in conventional metals and semiconductors where the energy spectrum can be approximated by a parabolic (free-electron-like) dispersion relation.

1.2 Graphene Nanoribbons

Graphene nanoribbon (GNR) is a nano size piece of graphene which is cut in a specific geometry with aspect ratio $\left(= \frac{\text{length}}{\text{width}}\right)$ greater than one. The two famous nanoribbons of Graphene are schematically shown in figure 1.3 below. The width of armchair like GNR can be decided by counting the number of dimer lines (N_a) on the other hand the width of

zigzag like GNR can be determined by counting the number of zizag chains as depicted in figure 1.3 (a) and (b). However, this thesis focuses only on zigzag graphene nanoribbon (ZGNR) because of the FM nature of the zigzag edges [8].

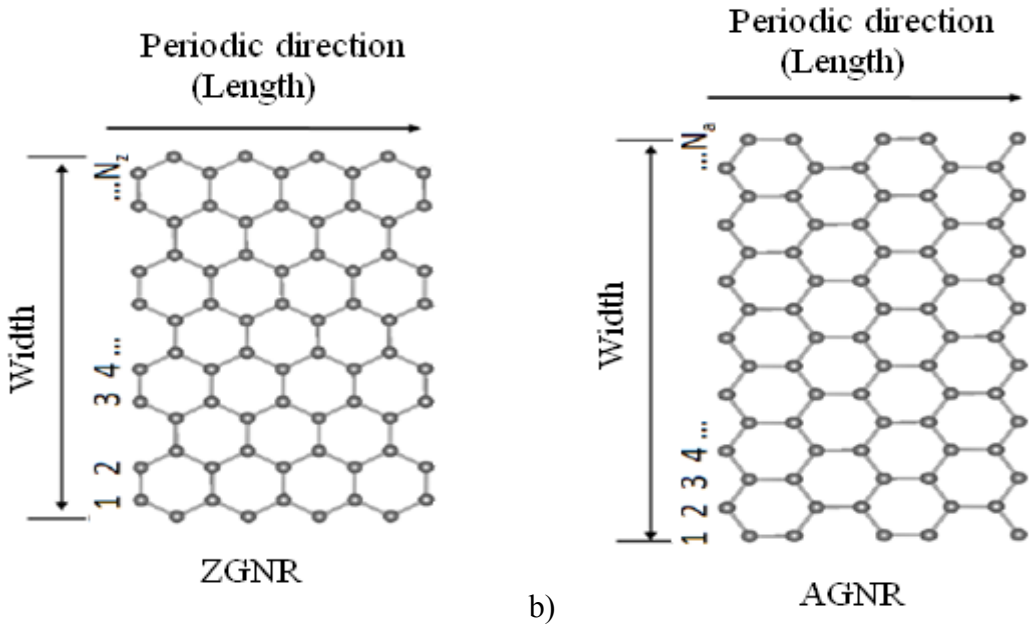

Figure 1.3 (a) Structure of zigzag graphene nanoribbon (b.) Structure of armchair graphene nanoribbon [9].

1.2.1 Electronic and Magnetic Properties of ZGNRs

For nanoribbons with zigzag shaped edges, without considering spin states, DFT calculations have shown that a set of doubly degenerate flat edge-state bands is present at the Fermi-level (E_F) [10], which give rise to high density of states (DOS) at E_F as depicted in the figure 1.4. This DOS peak at E_F is half filled, which therefore provides ferromagnetic instability leading to magnetic states.

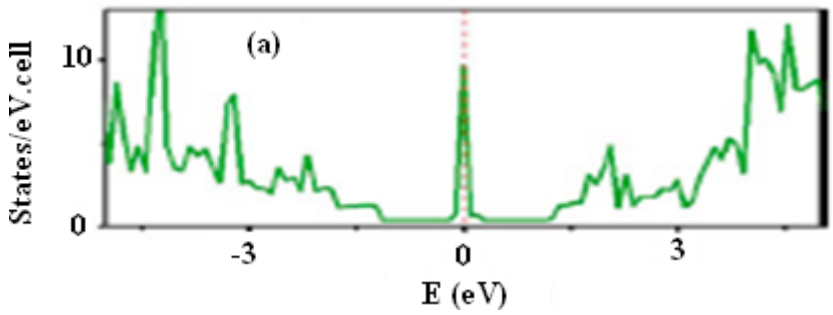

Figure 1.4 Density of States (DOS) plot for NM States of 8ZGNR [8]

By inclusion of the spin degrees of freedom within DFT methods, the zigzag GNRs have been predicted to have a magnetic insulating ground state with ferromagnetic ordering at each zigzag edge, and antiparallel spin orientation between the two edges that induces perfect antiferromagnetic (AFM) character in the ZGNRs [8]. Thus note that in ZGNRs the spin moments are mainly distributed at the edge of carbon atoms.

1.3 Half-Metallicity

1.3.1 Definition: It is the property of materials with non-equilibrium spin density in which one spin channel is conducting while the other spin channel remains semi-conducting or insulating as shown in the figure 1.5. One brilliant example occurs in the zigzag GNR which is proved to be half metallic by applying strong in-plane transverse electric field and by decorating the edges with chemical function groups. Other than ZGNR, heusler alloys, diluted manganites, chromium arsenide, chromium oxide, etc are some of the novel candidate half metals.

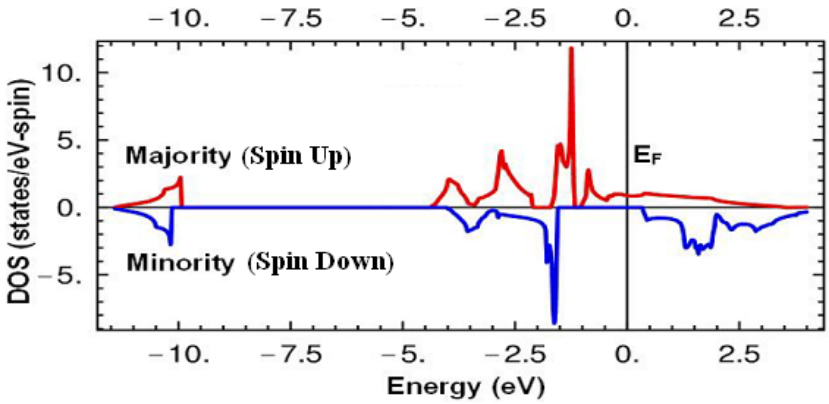

Figure 1.5 The density of states (DOS) spectrum for half metallic CrAs [11]

1.3.2 Half-Metallicity in ZGNR

Recent ab initio calculations have shown that the graphene nanostructures can be a good half metallic conductors, especially the zigzag graphene nanoribbon which already have the proven conductivity and very low energy gaps on passivations [6]. It is anticipated that the carbon atoms present at the edges with zigzag nature in the ribbons are the main contributors towards half metallicity

1.3.2.1 Electric Field

It has been stated that zigzag GNRs are zero-gap semiconductors with two localized electronic edge states. These two states are ferromagnetically ordered at each edge, and antiferromagnetically coupled with each other, which means the total spin of zigzag GNRs is zero. Since these states are edge states, the effects of external transverse fields are expected to be significant. Son and his group have investigated the aforementioned problems by performing DFT calculations [2]. In their research, the external transverse

fields are simulated by a periodic saw-tooth-type potential, which is perpendicular to the direction of the ribbons edge. Taking n =16 as a representative model, Son found that the valence and conduction bands associated with one spin orientation become closer, and eventually this proximity closes the gap under strong enough external electric fields. Whereas band gaps of the other spin orientation are widen. As shown in the figure 1.6 below, spin-degenerate band structures become spin-selective and eventually changed into half metals by applying external electric fields.

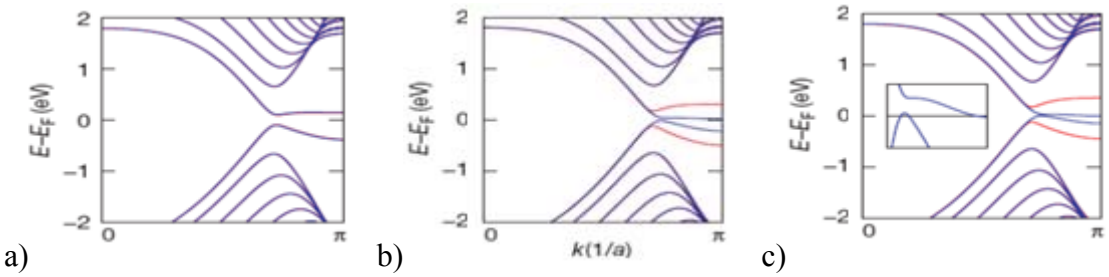

Figure 1.6 from left to right, the spin-resolved band structures of zigzag GNRs with n = 16 under electric fields of a) 0.0, b) 0.05 and c) 0.1 V/Å, respectively. The red and blue lines denote bands of different spin channels the inset show the spin band gap opening by zooming up spin band structure [2].

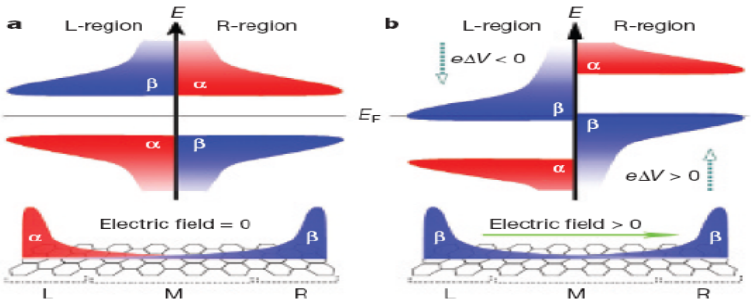

Figure 1.7 (a) Schematic density-of-states diagram of the zigzag GNRs without external electric field. L-region (R-region) means the left (right) side of GNRs, and α

and β are two spin channels. (b) Density-of-states diagram under applied electric field [2].

The half-metallic property also originates from the fact that the applied electric fields induce energy- level shifts of edge states. Based on the analysis of density of states, Son et al. have used a simple model to explain the appearance of half-metallic property. As shown in figure 1.7(a) above, the spin-polarized states localized at two edges (left and right edges) are spatially well separated and degenerate in energy when the electric fields are not applied. Since both occupied and unoccupied states of one special spin channel are located at the opposite sides of the zigzag GNRs, the effect of external electric field on them is different, namely, raising the energy-level of occupied states, while lowering the one of unoccupied. Consequently, the energy gaps of one spin channel will be closed by external electric field, while leaving the other ones as insulating. Thus, the half-metallicity comes from the relative movement in energy of edge states under electrostatic potential. The electric field range at which zigzag GNRs remain half-metallic increases with the ribbon width. All these results indicate that the half-metallicity induced by electric fields is robust, and independent on the theoretical methods adopted. Thus, the only problem is how to overcome the obstacle of high critical electric field in applications.

1.3.2.2 Chemical Doping

Half-metallicity can also be achieved with anti-symmetrical potential at two edges, doping boron and nitrogen atoms in zigzag GNRs is one of the possible ways to achieve this effect. Kan and his group have proposed one interesting model, as shown in figure

1.8 below [12]. BN chains are integrated into zigzag GNRs, and each BN chain is well separated by n carbon chains (n = 1, 2, 3). It is known that, boron and nitrogen atoms provide holes and electrons when they are separately doped into zigzag GNRs. Therefore, the effect of boron and nitrogen atoms on the edge states definitely is different, which may induce half-metallicity.

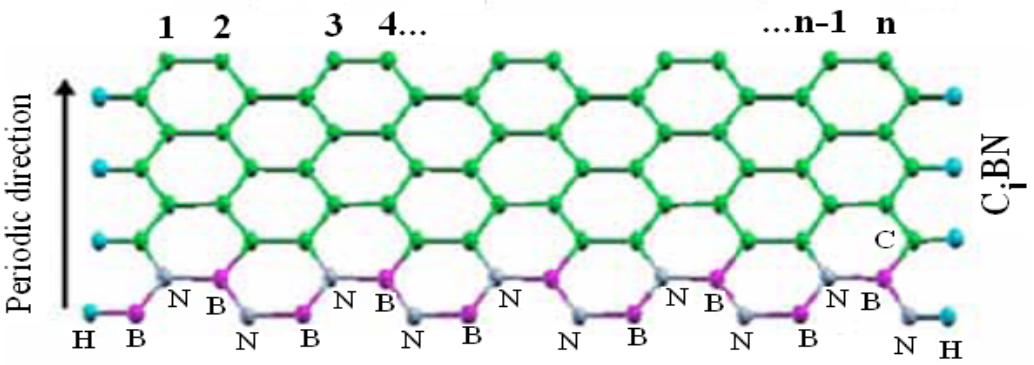

Figure 1.8 The atomic structures of differentially doped nanoribbons. Green, pink, gray, and sapphire balls denote carbon, boron, nitrogen, and hydrogen atoms, respectively [12].

To confirm their proposal, they carefully studied the electronic structures of such hybrid BCN nanoribbons with DFT methods. There are three significant characters: firstly, all studied hybrid BCN nanoribbons, namely, C_1BN, C_2BN, and C_3BN, are spin-selective materials when n is larger than 8. Secondly, all the studied BCN nanoribbons become half metals with enough width of ribbons. Thirdly, the critical width realizing half-metallicity is different. For C_1BN, the critical width is n = 12, while 10 and 8 for C_2BN, and C_3BN, respectively. In another words, the critical width decreases with the increasing of intervened carbon chains. These results mean that half-metallicity in hybrid BCN ribbons can be easily realized by controlling the doping methods of BN chains. Similarly,

Dutta and his group have proposed that doping boron and nitrogen atoms into zigzag GNRs can lead to half-metallicity [13]. Slightly different with Kan's group idea, the Dutta's group suggested that doped BN chains are perpendicular to the periodic direction. However, the electronic behaviours of doped BN chains are similar with the reported results of Kan and his group.

In another way, Zheng and his group have investigated the nature of the edge states in the valence and conduction bands by simulating the contour of wave functions of the valence and conduction bands as shown in figure 1.9 below, and proposed how half-metallicity is achieved upon doping B and N [14].

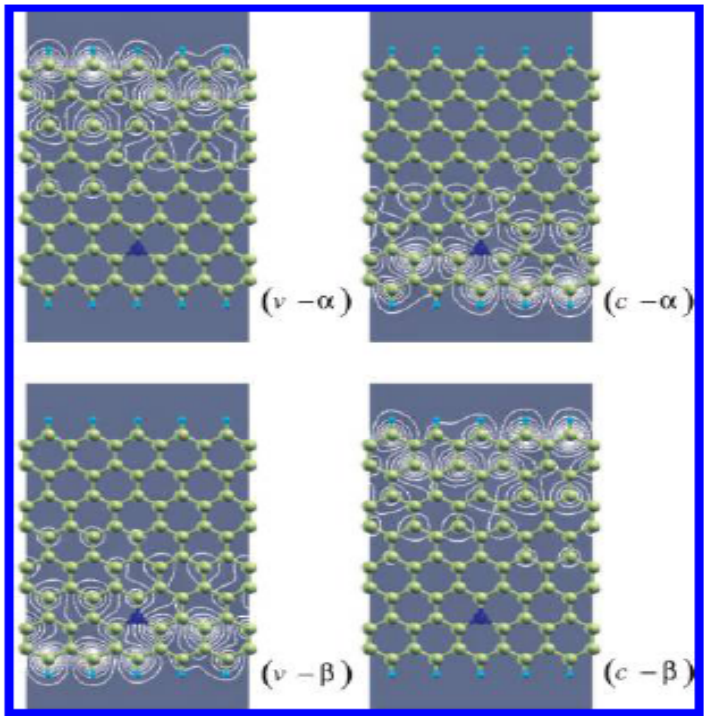

Figure 1.9 Contour of wave functions (edge states) of the valence bands and conduction bands at the Γ point for the undoped 8ZGNR. v means valence bands, while

c means conduction bands. α and β are the spin indices for spin up and spin down. The carbon atom shown in blue indicates one of the possible doping sites [14].

It can be seen from the figure 1.9 that, in zigzag GNRs, the wave functions with α spin in the valence bands are localized at the top edge while those with β spin are localized at the bottom edge. On the opposite, in the conduction bands, the wave functions with α spin are localized at the bottom edge while those with beta spin are localized at the top edge. Thus, if two carbon atoms on opposite sides (bottom and top edges) are replaced by one B and one N atom, the demands for electron or hole in both the B doping and the N doping schemes to shift the Fermi level can be satisfied and as a result full half metallicity is induced to the zigzag GNR [14].

1.3.3. Spin Polarization as a Measure of the Half-Metallicity

The spin polarization is defined as the ratio of the majority and minority spin density of states at a Fermi level, $P = \frac{DOS_{Maj} - DOS_{Min}}{DOS_{Maj} + DOS_{Min}}$. As shown in figure 1.10 below, since the density of states of majority spin states (in this case up-spin electrons) and minority spin states (down-spin electrons) are equal in paramagnetic materials, P=0 for paramagnetic materials. On the other hand, since the density of state of spin up and down-spins are different in ferromagnetic materials, P is larger than 0, but smaller than 1 for ferromagnetic materials. The P values of Fe and Co are known to be around 0.5. If a material has a band gap in the minority band (semiconducting) at a Fermi level and exhibits metallic behavior in the majority band, the density of state of the minority band

is zero at the Fermi level. In this case, since only up-spin electrons are present at the Fermi level, P=1. This type of material is called **"half-metal"** because it exhibits both metallic and semiconducting behaviors.

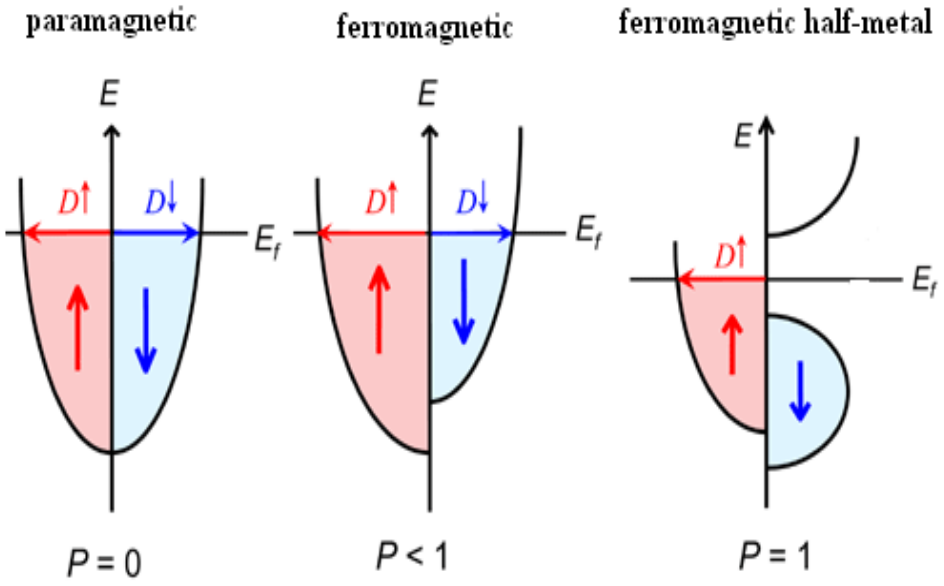

Figure 1.10 Density of states of paramagnetic, ferromagnetic and ferromagnetic half metal [15]

1.3.4 Applications

Half metals hold the promise for spintronic applications [16]. Spintronics is a multidisciplinary field whose central theme is the active manipulation of spin degrees of freedom in solid-state systems. The ability to manipulate and detect spin offers the potential of a new paradigm for electrical devices. It has been suggested that adding the spin degree of freedom to conventional charge-based electronic devices or using spin alone has the potential advantages of non-volatility, increased data processing speed,

decreased electric power consumption, and increased integration densities compared with conventional semiconductor devices [17].

1.3.4.1 Magnetoresistance

Magnetoresistance (MR) refers to a change in the electrical current when the relative magnetization of the ferromagnetic layers changes their alignment [18]. For half metals the MR value could be expressed as $MR = \frac{2P^2}{1-P^2} * 100\%$, where P is spin polarization. Hence, as far as polarization is 1 for half metals, the MR value is infinity. There are two major types of magnetoresistance effects, the tunneling magnetoresitance(TMR) and the giant magneto resistance (GMR) effects. The TMR effect is also observed when a thin insulator layer is sandwiched between two ferromagnetic layers [19]. While the GMR effect is observed when we form several layers of feromagnet/normal metal (FM/NM) interfaces.

CHAPTER TWO

2. Objectives

2.1. General Objective:

- To get a specific conformation of graphene nanoribbons with half metallic behavior by the application of ab initio (or first principle) techniques.

2.2. Specific Objectives:

- To model and simulate various useful doped and undoped conformations of graphene nanoribbon.
- To investigate the charge carrier density and spin transport properties of the newly determined graphene nanoribbon conformations with the help of first principle techniques.

CHAPTER THREE

3. Methodologies

Modeling and simulation has been performed by the ab-initio SIESTA code. The ab-initio techniques like DFT, and LSDA within the SIESTA code are employed to investigate the electronic structure and transport properties of the system. Before we proceed to the details about the software and the ab-initio techniques, it is appropriate to define our system.

3.1. The Many Body System

Our system is defined to be a many body system which could well be described by the many body Hamiltonian. And simulating the physical properties of such systems is just solving the many-body Schroedinger equation of the systems.

The Hamiltonian of a typical many-body system can be written as:

$$H = T + T_n + V_{int} + V_{nn} + V_{ext} \tag{3.1}$$

When decomposed term by term, we get the following expressions:

$$T = \frac{\hbar}{2m_e}\sum_i \nabla_i^2 \tag{3.2}$$

Where T is the electron kinetic energy;

m_e = mass of electron

$$T_n = -\sum_I \frac{\hbar^2}{2M_I}\nabla_I^2 \tag{3.3}$$

Where T_n is the nuclei kinetic energy;

M_I = mass of nuclei

$$V_{int} = \frac{1}{2}\sum_{i \neq j} \frac{e^2}{|r_i - r_j|} \tag{3.4}$$

Where V_{int} is the electron-electron repulsion term;

r_i (r_j) = positions of electrons

$$V_{nn} = \frac{1}{2}\sum_{I \neq J} \frac{Z_I Z_J e^2}{|R_I - R_J|} \tag{3.5}$$

Where V_{nn} is the nuclei-nuclei repulsion term;

R_I, R_J = positions of nuclei

Z_I, R_J = nuclear charge

$$V_{ext} = -\sum_{i,I} \frac{Z_I e^2}{|r_i - R_I|} \tag{3.6}$$

Where, V_{ext} is the attractive interaction term between the electrons and the nuclei described as an external potential for the electrons.

3.2. First Principle Calculations (Ab-Initio Techniques)

The above many body Hamiltonian that describes our system can be calculated using ab initio techniques. Ab-initio is a Latin term meaning “from the beginning” [20] or “from scratch”. This technique does not employ any experimental data to reach at the approximate solution of the many body Schroedinger equation (or the many body Hamiltonian). Because it is impossible to reach at the exact solution of the many body Schroedinger equation (many body Hamiltonian), the ab-initio techniques employ various

theories and approximations to reach at the approximate solution of the many body Hamiltonian.

Born-Oppenheimer Approximation

Born-Oppenheimer (adiabatic) approximation is basically setting the mass of nuclei to infinity. Since mass of nuclei is immensely larger than mass of electron. Thus when dealing with electron-nuclei many body systems, the kinetic energy of the nuclei can be ignored. Adiabatic approximation reduces the number of degrees of freedom of the system so all the contribution from nuclei interactions (V_{nn}) is now nothing but a constant.

3.3 Density Functional Theory

Density functional theory states in general that any property of a many interacting system can be described in terms of the ground state density $n_0(r)$ where $n_0(r)$ is a scalar function of position. Thus in principle, a functional of the ground state density determines all the information for the ground state and excited states.

Hohenberg-Kohn Theorems

In 1964 Hohenberg and Kohn proposed two theorems to formulate density functional theory as an exact theory of many-body systems [21]. These theorems are commonly accepted as the onset of modern DFT. The two theorems are:

Theorem I: For any system of N-interacting electrons, any of its physical properties are completely determined by the ground state electron density n(r).

Theorem II: The global minimum of energy functional is the ground state energy, and the corresponding electron density is the ground state density.

The Hamiltonian of many-body system can be written as:

$$H = -\frac{\hbar^2}{2m_e}\sum_i \nabla_i^2 + \sum_i v_{ext}(r_i) + \frac{1}{2}\sum_{i\neq j}\frac{e^2}{|r_i - r_j|} \qquad (3.7)$$

And the energy functional can be expressed as:

$$E_{HK}[n] = T[n] + E_{int}[n] + \int drV_{ext}(r)n(r) + E_{II} = F_{HK}[n] + \int drV_{ext}(r)n(r) + E_{II} \qquad (3.8)$$

Where E_{II} is nucleus-nucleus interaction, $F_{HK}[n]$ is system internal energy, including electron kinetic, potential and interaction energy. So if we know $F_{HK}[n]$ then we can determine the electron density of the ground state by simply minimizing the energy functional.

The Kohn-Sham Equations

DFT is in principle an exact theory. However, it has a draw back; the exact energy functional is not known. So one needs to adopt schemes for obtaining an expression for the energy functional that can later be used in the computations. In 1965, Kohn and Sham [22] proposed to replace the original many-body problem by an auxiliary independent-particle problem with all the interactions between electrons are classified into an exchange-correlation term. The following are the Kohn-Sham equations.

$$(H_{KS}^{\sigma} - \varepsilon_i^{\sigma})\psi_i^{\sigma}(r) = 0 \qquad 3.9$$

Where ε_i^σ are Kohn-Sham eigenenergies. And H_{KS}^σ is the effective Hamiltonian

$$H_{KS}^\sigma(r) = -\frac{1}{2}\nabla^2 + V_{KS}^\sigma(r) \tag{3.10}$$

Where V_{KS}^σ is Kohn-Sham potential and it is defined as

$$V_{KS}^\sigma(r) = V_{ext}(r) + \frac{\delta E_{Hartree}}{\delta n((r),\sigma)} + \frac{\delta E_{XC}}{\delta n((r),\sigma)} \Rightarrow V_{KS}^\sigma(r) = V_{ext}(r) + V_{Hartree}(r) + V_{XC}^\sigma(r) \tag{3.11}$$

These equations must be solved with in a self consistent basis. Also the Kohn-Sham equations are independent of any approximation to the exchange correlation energy functional $E_{xc}[n]$. Thus, Kohn and Sham devised the following imperative procedures to solve the above equations:

1. Initial guess for density $n^\uparrow(r), n^\downarrow(r)$
2. Calculate Kohn-Sham potential $V_{KS}^\sigma(r)$
3. Solve Kohn-Sham equations (1) and (2)
4. Calculate electron density $n^\uparrow(r), n^\downarrow(r)$ using the density equation, $n(r) = \sum_\sigma n(r,\sigma) = \sum_\sigma \sum_{i=1}^{N^\sigma} \left|\psi_i^\sigma(r)\right|$; Where ψ_i^σ is the i^{th} single particle orbital with spin component σ.
5. Repeat step 2 until $n^\uparrow(r), n^\downarrow(r)$ is converged.

3.4 Local (Spin) Density Approximation, L(S)DA

LDA is a simple approximation assuming that the electron density is only slightly modulated by the potential of the ion cores.

Thus the exchange-correlation functional is given by [23]:

$$E_{XC}^{LDA}[n^{\uparrow}, n^{\downarrow}] = \int d^3 r n(r) \varepsilon_{XC}(n^{\uparrow}(r), n^{\downarrow}(r)) \tag{3.12}$$

Where $\varepsilon_{XC}(n^{\uparrow}(r), n^{\downarrow}(r))$ is the exchange-correlation energy per particle for a homogeneous electron gas with density n(r) and can be split into two as:

$$\varepsilon_{XC}(n^{\uparrow}(r), n^{\downarrow}(r)) = \varepsilon_X(n^{\uparrow}(r), n^{\downarrow}(r)) + \varepsilon_C(n^{\uparrow}(r), n^{\downarrow}(r)) \tag{3.13}$$

The exchange part for the homogeneous electron gas can be calculated with Hartree-Fock method as:

$$\varepsilon_X(n^{\uparrow}(r), n^{\downarrow}(r)) = -\frac{1}{2^{2/3}} \frac{3}{8} e^2 \left(\frac{3}{\pi}\right)^{\frac{1}{3}} ((n^{\uparrow}(r))^{\frac{1}{3}} - \frac{1}{2^{2/3}} \frac{3}{8} e^2 \left(\frac{3}{\pi}\right)^{\frac{1}{3}} ((n^{\downarrow}(r))^{\frac{1}{3}} \tag{3.14}$$

The calculation of the correlation term $\varepsilon_C(n^{\uparrow}(r), n^{\downarrow}(r))$ is more difficult to calculate. Using Monte Carlo method [24] it may be computed accurately. The LDA has been quite successful in describing ground state properties of materials with small variations in the electronic density e.g. metallic systems. When there are strong local density gradients the LDA is not an effective approximation. Also, the band gaps in semiconductors and insulators are usually underestimated by 40% which is a common observance in all the variational techniques and DFT is not an exception.

3.5 Two-Probe system

A two-probe system is a system made up of two contact leads (electrodes) attached to the sample (central region) to be tested. One of the leads, mostly the left lead, is used for charge carrier injection while the other one, mostly the right lead, is used for charge

carrier collection. The two electrodes are semi-infinite in nature and are perfectly metallic.

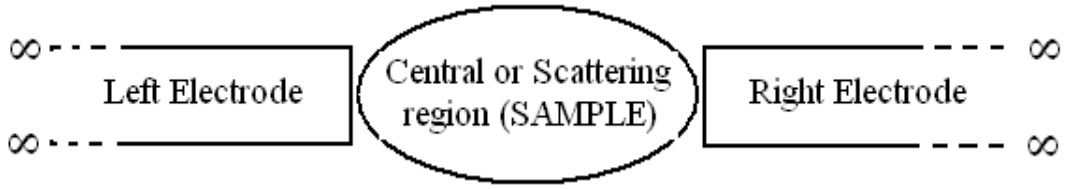

Figure 3.1 Two-Probe System

In preparing a two-probe device (system), materials which could be used as electrode are Gold metal to inject electrons, Silver metal injects electrons, Aluminum injects holes, Graphene nanoribbons, and other useful device electrodes are Carbon Nano Tubes (CNTs), Atomic chains and Half metallic electrodes (e.g., Fe, CrO2), etc.

The contact preparation is the most important task of device fabrication. Because a slight distance in between sample and electrode can kill the charge carrier transmission and make the device useless. The ideal distance between them is the equilibrium bond length of the surface atoms of electrode and sample.

3.6. SIESTA

SIESTA (Spanish Initiative for Electronic Simulations with Thousands of Atoms) is both a method and its computer program implementation, to perform electronic structure calculations and ab initio molecular dynamics simulations of molecules and solids [25]. Its main characteristics are:

- It uses the standard Kohn-Sham self-consistent density functional method in the local density (LDA-LSDA) or generalized gradient (GGA) approximations which are explained in the preceding sections of this chapter.
- It uses atomic orbitals as a basis set, allowing unlimited multiple-zeta and angular momenta, polarization and off-site orbitals.
- Projects the electron wave functions and density onto a real-space grid in order to calculate the Hartree and exchange-correlation potentials and their matrix elements.
- It is written in Python programming language and memory is allocated dynamically.

3.7 ATK/VNL

ATK/VNL are the interfaces of SIESTA.

Atomistix ToolKit (ATK) is a software package that offers unique capabilities for simulating electrical transport properties of nanodevices on the atomic scale. Based on an open architecture which integrates a powerful scripting language with a graphical user interface, ATK is a comprehensive platform for studies in nano-electronics, using methods that range from both accurate quantum-mechanical first-principles and fast semi-empirical methods to classical potentials for very fast geometry optimizations and molecular dynamics calculations. A special focus is placed on treating large-scale systems, with several thousand atoms. Moreover, ATK includes a very advanced electrostatic model to allow realistic simulations of nanoscale transistor structures. ATK

also offers basic electronic structure calculations, including geometry optimization, of molecules and periodic structures like bulk crystals, nanotubes, slabs, etc.

Virtual NanoLab (VNL) offers a rich set of powerful tools for investigating and analyzing the properties of nanostructures by simulating measurements through numerical calculations. It gives scientists, engineers, and researchers access to powerful atomic scale modeling tools. VNL provides convenient programs to

- design and build several types of nanostructures
- setup scripts for performing calculations
- inspect, analyze, and visualize your results

Numerical calculations in VNL is processed by the Atomistix ToolKit (ATK), which combines advanced numerical methods, such as density-functional theory (DFT) and non-equilibrium Green's functions (NEGF), to describe the detailed electronic structure of nanoscale devices.

The most unique capability of VNL is the ability to investigate the electronic transport properties of nanoscale devices. Advanced numerical algorithms enable the application of a bias voltage across the structure, as well as the calculation and analysis of current-voltage characteristics of so-called two-probe systems. In two-probe systems, two electrodes (macroscopic conductors such as metal surfaces, carbon nanotubes, nanowires or atomic chains) are coupled by a nanoscale central region, which may be a molecule, a nanotube (between metal surfaces, for instance), or an interface between two materials. It is therefore possible to use VNL to study how the conductance of a carbon nanotube

changes due to an adsorbed molecule, the electronic transport properties of molecular electronic devices, or atomic-scale wires. In addition, a special tool for constructing special two-probe devices called magnetic tunnel junctions is also part of VNL. The design of VNL allows non-experts in quantum chemistry and electronic structure calculations to use the advanced methods implemented in ATK; this design approach allows you to focus on the physical properties of the systems, and let the program handle the details of the numerical models.

Thus, the SIESTA based ATK/VNL package offers the spectrum of tools for

- Building and setting up molecule, bulk, and two-probe systems.
- Specify the physical properties that should be calculated for a given system.
- Define parameters for fine tuning the density-functional theory (DFT) and non-equilibrium Green's function (NEGF) calculations.
- Generate and execute NanoLanguage Scripts.
- Inspect, analyze and visualize the results of your calculations.

All the VNL tools are explained in the table below.

Table 3.1. The Virtual Nano Lab (VNL) Tools and Corresponding Descriptions [25]

Tools	**Icon**	**Description**
Crystal Cupboard		Database of bulk systems

Atomic Manipulator		Set up two-probe systems and make modifications to magnetic tunnel junctions.
Molecular Builder		Enables to build and construct molecules ready to be used in other VNL tools
Bulk Builder		Enables to build and construct bulk systems ready to be studied and analyzed with other VNL tools
NanoLanguage Scripter		Create complete calculation set-ups and store these as NanoLanguage scripts
Method Editor	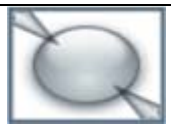	Predefine DFT and NEGF parameters for re-use in the NanoLanguage Scripter when generating NanoLanguage scripts.
Sript Editor		Manually edit and extend NanoLanguage scripts constructed by the different set of VNL tools

3.8 Sample Preparation

In this thesis half metallic conformations are investigated in two ways such as doping the ribbon at specific sites, which is known as half edge doping and creating vacancy inside the ribbon. For these activities two different small width ribbons are selected considering our computational power and capacity. i.e., 2ZGNR is selected for doping and 3ZGNR is

selected for creating the vacancy where values of n are 2 and 3 respectively. The VNL tools shown in Table 3.1 above, especially, the Script Editor, Bulk Builder and Atomic Manipulator tools are used for sample preparation. In preparing respective two probe systems of the samples, the sample ribbon itself is used as electrode and the width of the central region is maintained at 1.35Å for the doped (decorated) ribbons and at 1.2285Å for the ribbon with vacancy.

The following are the ribbons used for doping and creating the vacancy.

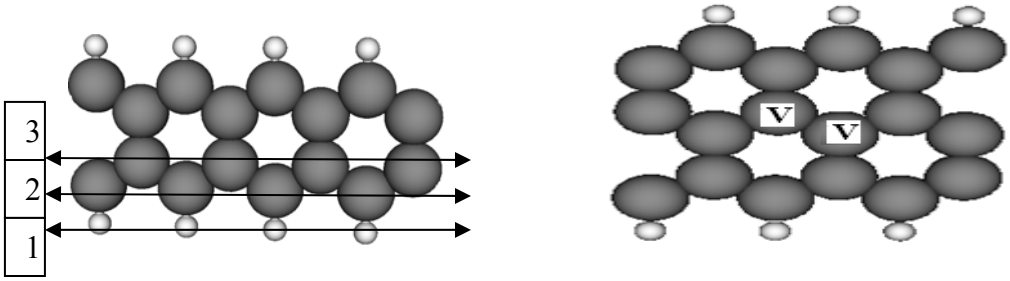

a) **b)**

Figure 3.2 Schematic diagrams of a) 2ZGNR for doping b) 3ZGNR for vacancy

The dopants used are Boron (B), Nitrogen (N) and Oxygen (O). The bottom zigzag edge as well as the bottom hydrogen sites depicted in figure 3.2(a) is dedicated to boron doping while the top zigzag edge and the top hydrogen sites are for Nitrogen or Oxygen doping. More specifically, the numbered arrows indicate the doping sites. And the letter 'V' in figure 3.2(b) indicates the two possible sites for creating vacancy. The devices (two probe systems) modeled using the ribbons in figure 3.2(a) and (b) are categorized in five groups as shown in the figure 3.3. The first group consists of the reference 2ZGNR and 3ZGNR two-probe samples (devices) which are fully Hydrogen saturated; the second

group consists of Boron doped 2ZGNR two- probe samples (devices); the third group consists of Boron-Nitrogen doped 2ZGNR two-probe samples; the fourth group consists of Boron-Oxygen doped 2ZGNR two-probe samples (devices) and the fifth group consists of 3ZGNR with vacancy two-probe sample (device).

Category 1 – References (2ZGNR and 3ZGNR) two probe devices:

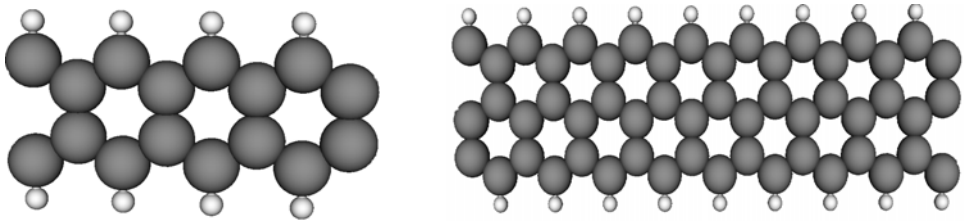

a) **Device A** **Device B**

Category 2 - Boron doped two probe devices:

The conformation (1), the superscript, stands for replacing H passivents by B atoms. The conformation (2) stands for replacing outer C atoms of the zigzag edge by B atoms and the conformation (3) represents replacing of inner C atoms of zigzag edge by B atoms.

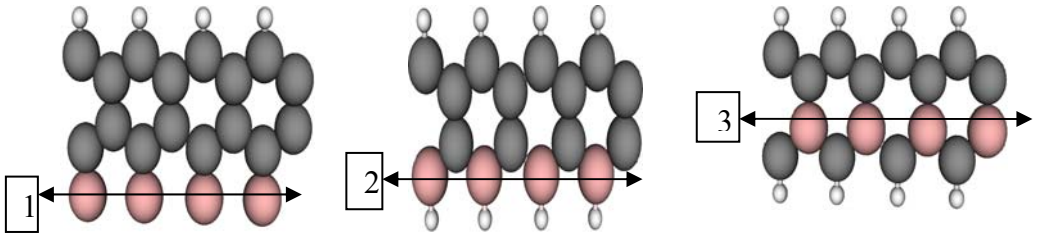

b) A^1_B A^2_B A^3_B

Category 3 - Boron-Nitrogen doped two probe devices:

The conformations 1, 2, 3 have their usual meanings for B and N atoms.

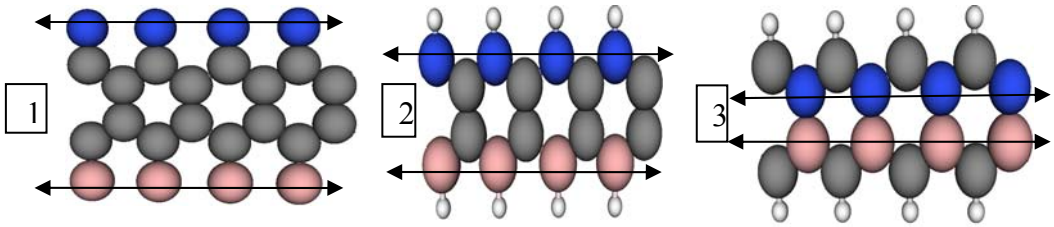

c) A^1_{BN} A^2_{BN} A^3_{BN}

Category 4 - Boron-Oxygen doped two probe devices:

The conformations 1, 2, 3 have their usual meaning for B and O atoms

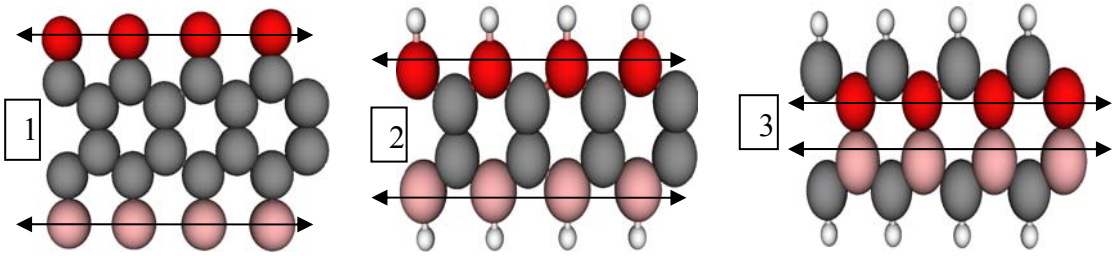

d) A^1_{BO} A^2_{BO} A^3_{BO}

Category 5 - 3ZGNR two probe device with vacancy:

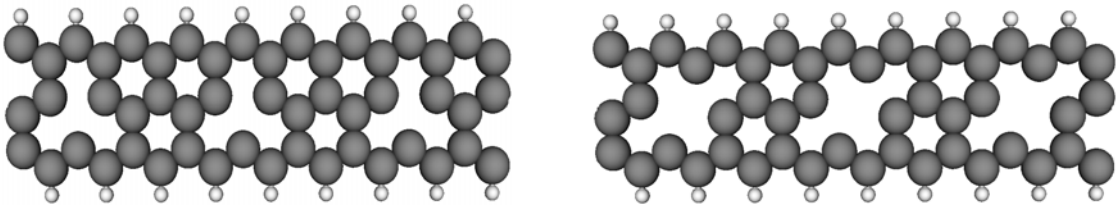

e) B^1_V B^2_V

Figure 3.3 Samples a) Reference devices b) Boron doped 2ZGNR [carbon – grey, boron – pink and hydrogen - white]; c) Boron-Nitrogen doped 2ZGNR [carbon – grey,

boron – pink, nitrogen – blue and hydrogen - white]; d) Boron-Oxygen doped 2ZGNR [carbon – grey, boron – pink, oxygen – red and hydrogen - white] and e) 3ZGNR with vacancy [carbon – grey and hydrogen - white].

Table 3.2 Sample Device Descriptions

Sample Device	**Device Description**
A	Sample reference device formed from fully hydrogen saturated 2ZGNR.
B	Sample reference device formed from fully hydrogen saturated 3ZGNR.
A^{1}_{B}	Boron doped 2ZGNR device where Boron is doped at site 1 (bottom hydrogen sites).
A^{2}_{B}	Boron doped 2ZGNR device where Boron is doped at site 2 (bottom zigzag edge).
A^{3}_{B}	Boron doped 2ZGNR device where Boron is doped at site 3 (same bottom zigzag edge but different sublattice)
A^{1}_{BN}	B – N pair doped 2ZGNR device where the impurity atoms, Boron and Nitrogen, are doped at site 1 bottom and top hydrogen sites respectively.
A^{2}_{BN}	B – N pair doped 2ZGNR device where Boron and Nitrogen are doped at site 2 bottom and top zigzag edges.
A^{3}_{BN}	B – N pair doped 2ZGNR device where Boron and Nitrogen are doped

	at site 3 bottom and top zigzag edges.
A^1_{BO}	B – O pair doped 2ZGNR device where Boron and Oxygen are doped at site 1 bottom and top hydrogen sites respectively.
A^2_{BO}	B – O pair doped 2ZGNR device where Boron and Oxygen are doped at site 2 bottom and top zigzag edges.
A^3_{BO}	B – O pair doped 2ZGNR device where Boron and Oxygen are doped. at site 3 bottom and top zigzag edges
B^1_V	Device made from 3ZGNR where one carbon atom is removed to form the vacancy.
B^2_V	Device made from 3ZGNR where two carbon atoms are removed to form the vacancies.

N.B:

- Sites 2 and 3 are on same zigzag edge but different sublattices.

3.9 Computational Details

The doping as well as the vacancy effects in ZGNRs are analyzed by performing density functional theory calculations using the SIESTA code. The wave function is expanded with a Single Zeta basis set, and the exchange-correlation potential is treated at the level of Local (Spin) Density Approximation (LDA.PZ). The fineness of real space grid is determined by an equivalent plane wave cutoff 150 Ryd. The Brillouin zone is sampled by a $1 \times 1 \times 20$ *k*-point grid. Geometry optimization is done with force tolerance of

0.55eV/Å. We begin with doping only boron atom and extend our investigation to B-N and B-O pairs doping end up with the vacancy devices.

Table 3.3 Summary of Simulation Parameters Set at the Method Tab in the Nano Language Scripter Tool of VNL

Simulation Parameters	**Set (Adjusted)**
Geometry optimization: Force tolerance	Quasi Newton 0.55 eV/Å
Basis Set	Single Zeta
Brillouin zone integration (k-points A, B, C)	1, 1, 20
Eigen state occupation parameters: Electron temperature for left electrode Electron temperature for right electrode	 300K 300K
Electron density parameters: Mesh cutoff Initial spin	 150 Ryd 1
Exchage Correlation Functional	LDA.PZ
Gated Two-probe	Enabled and set as ±50mV and ±100mV
Iteration control parameters: Tolerance Maximum steps	 E^{-3} 200

CHAPTER FOUR

4. Results and Discussions

This chapter is dedicated to the discussions of the results we got upon simulation. Samples are modeled from a hydrogen saturated ribbon so that only edge states are tailored to investigate half metallic conformation. In modeling the devices (two probe systems), the ribbon itself is used as an electrode to get the advantage of symmetric alignment among the central region and the electrodes. Geometry optimization using Quasi Newton algorithm is performed for the doped devices. The doping and the vacancy effect on the ribbons is sufficiently investigated simulating the density of states (DOS) and the transmission spectrum (TS). Spin Polarization at the Fermi Energy is calculated from the simulated DOS of the models for explaining the half metallic conformations as well as to show the models (devices) applicability to spintronics. The stability of the half metallic conformations is cross-checked by simulating the total minimum energy.

We started our analysis by investigating the DOS and TS of the reference 2ZGNR sample ribbon which is perfect, pure raw symmetrically passivated and configured. Following this, we extend our discussion to the doped and the vacant ribbons. Upon analyzing the DOS and TS of individual models, low energy spin states in the range of -0.1eV to 0.1eV are considered. All the calculations performed are within the said energy range.

4.1 DOS and TS for the 2ZGNR Reference Sample (A)

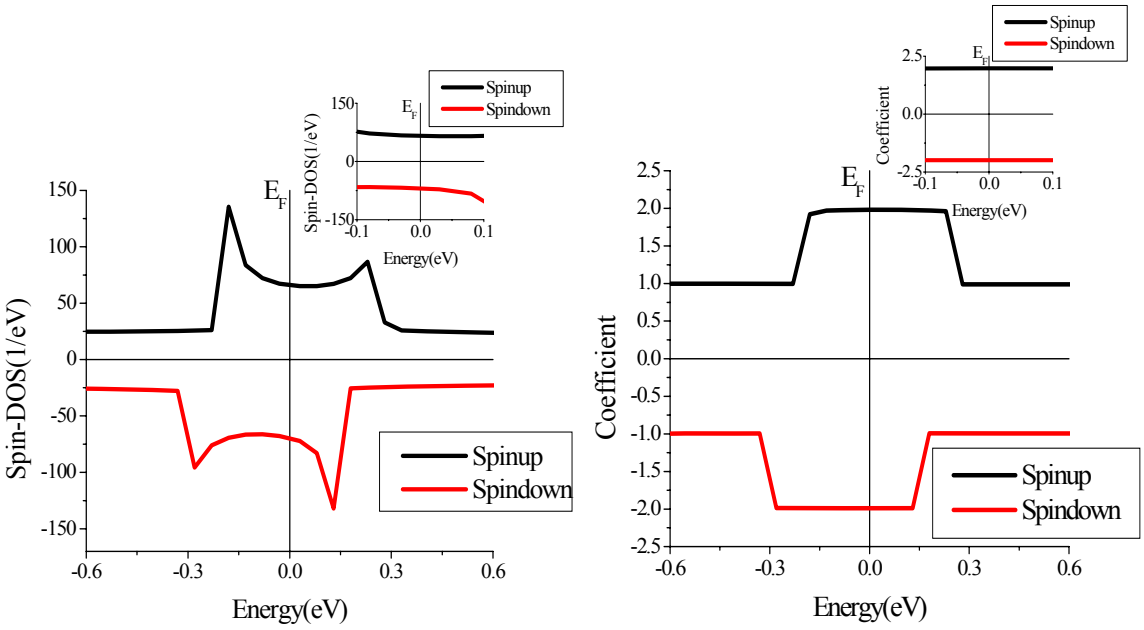

a) DOS **b) TS**

Figure 4.1 Schematic diagram of a) the density of states (DOS) spectrum of un-doped (bare) 2 ZGNR that is a standard reference for all the devices of type A with ribbon width of two zigzag raws. It shows a degeneracy in the low energy up and down spin states and b) its corresponding Transmission Spectrum (TS) showing a degeneracy in the low energy up and down spin channels. The inset figures represent the spin degeneracies for Dirac fermions of low energy states.

From the DOS spectrum as well as the Transmission Spectrum shown in figures 4.1(a) & (b) above, we can see that the up and down spin states are degenerate and are both conducting. By the word degeneracy we mean that the spin states around the Fermi level

are equal in amount. This degeneracy is due to the ferromagnetic alignment of atoms inside one edge and the anti-ferromagnetic alignment of atoms between two edges which results in a zero magnetic moment and non-spin polarized transport. Besides, to explain their degeneracy, if we observe the low energy states, i.e., states near the Fermi level of energies ranging from -0.1eV to 0.1eV, both up and down spin states cover equal area thus the states are exactly equal in number especially for the Dirac fermions as clearly seen from the inset of the figure 4.1(a), and they are also conducting. This result is more reinforced in the transmission spectrum (TS) as shown in the figure 4.1(b). It can be easily noticed from the TS curve that, the maximum coefficient is with magnitude of 1.99 for both up and down spin states and positioned at E_F, indicating that the low energy up and down spin states are equally conducting.

Hence, for now our aim is to break the low energy spin state degeneracy (i.e., to create unbalanced spin states around the Fermi level) and suggest a suitable spintronics device architecture to make one spin channel conducting and the other insulating so that half metallic devices are realized. Since we took fully Hydrogen saturated reference device, all the magnetism related or spin polarized properties in reference devices are directly related to the edge states which are localized at the edges. Therefore, we used chemical doping to further investigate the proposed half-metallic devices.

4.2 The Density of States (DOS) spectra for Boron Doped Ribbons (A_B)

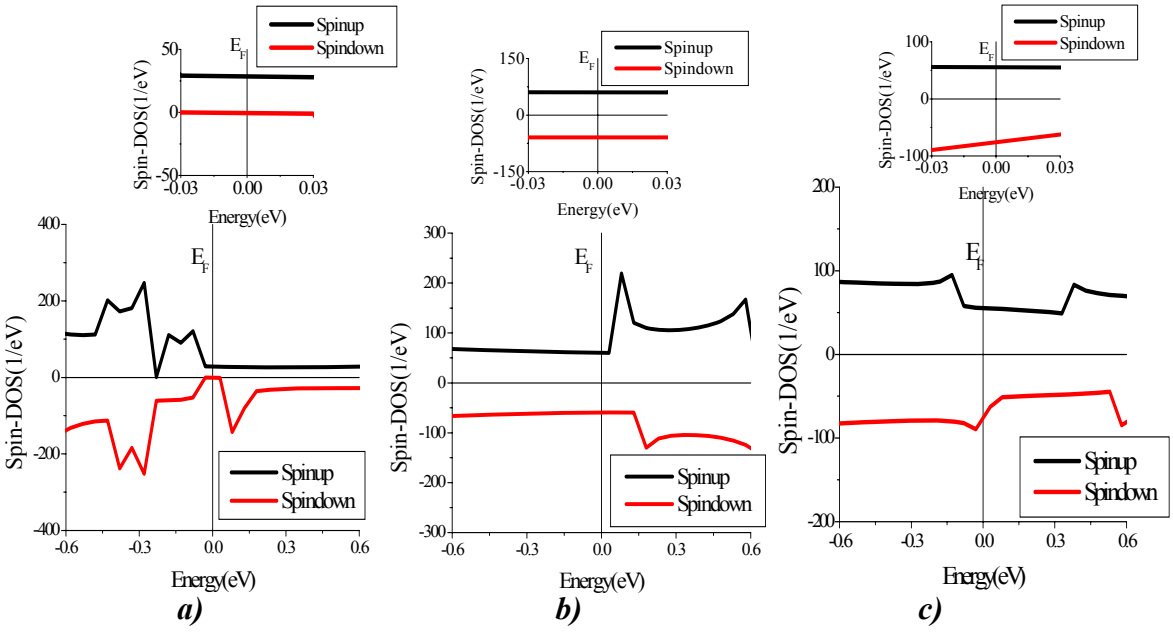

Figure 4.2 Density of States (DOS) spectra for devices a) A^1_B, b) A^2_B and c) A^3_B. The respective inset figures depict the spin for the Dirac fermions at very low energies.

From the DOS curve of device A^1_B shown in figure 4.2(a), around the Fermi level especially within the energy range -0.03eV to 0.03eV, the spin down states are almost zero while the spin up states show some significant amount within the same energy range indicating that spin is polarized around the Fermi level for this particular device. This fact is also observable from the inset of the figure 4.2(a) which indicates the total destruction of the spin degeneracy as the down spin electronic states are almost killed to zero value. Thus intending to get 100% polarized nature of Dirac fermions. Polarization (P) at E_F is calculated and found as 0.965 which shows the device is nearly half-metallic. As can be

seen from the DOS spectrum of figure 4.2(a), the majority spin states (spin up states) are more populated to the left of the Fermi level indicating that holes are the up spin carriers. This is truly expected as far as the boron doping is known for introducing holes to the device in general and to the central region in particular [14].

Similarly, in the density of states (DOS) spectrum of device A^2_B shown in the figure 4.2(b), closer to the Fermi level within the energy range -0.03eV to 0.03eV, we can see that the spin up and spin down states have insignificant difference in amount indicating that spin is unpolarized in this particular device. Polarization at E_F is calculated and found to be 0.002 which shows the device is paramagnetic which is also reflected from the inset of this figure.

On the other hand, for device A^3_B, the down spin states cover larger area near the Fermi level with in the same energy range. The majority spin states in this case are the down spin states and calculated polarization at E_F based on the DOS is found to be 0.156 which shows the device is ferromagnetic. The small amount of ferromagneticity is also reflected among the low energy electrons from the inset figure as the spin-degeneracy is prevalent among them

Table 4.1. Calculated polarization at E_F for devices A^1_B, A^2_B and A^3_B

Devices	**Up spin DOS ($D^{\uparrow}$)**	**Down spin DOS ($D^{\downarrow}$)**	**Polarization (P)**
A^1_B	28	0.5	0.965
A^2_B	60	59	0.008
A^3_B	55	76	0.160

The above results have shown that the Boron doping at different sites of the ribbon changes the magnetic behavior of the ribbon. i.e. the boron doping at the bottom hydrogen site converts the ribbon to nearly half metallic, while the boron doping on bottom zigzag edge but different sublattices converts the ribbon to be either paramagnetic or ferromagnetic.

Based on their low energy spin states, i.e., states at E_F, we can classify the above two spintronic devices as up spin selective and down spin selective devices. Using device A^1_B, we can inject $28 - 0.5 = 27.5 \approx 28$ low energy up spin states which makes it to be one of the best up spin injecting device. On the other hand, using device A^3_B, as long as down spin states are majority spin states at E_F, it enables us to inject 21 low energy down spin states.

Furthermore, to see the effect of boron doping at different sites of the ribbon, we have also calculated the charge densities for the top and bottom zigzag edges of the three devices A^1_B, A^2_B and A^3_B and compared with the previously discussed pure 2ZGNR reference devices.

Table 4.2. Total Charge Densities of Top and Bottom Zigzag Edges of devices A, A^1_B, A^2_B and A^3_B

Device	**Edges**	**q↑**	**q↓**	**q↑ + q↓**	**Differences**
A(reference device)	Top Zigzag Edge	8.302	8.132	16.434	0.0
	Bottom Zigzag Edge	8.302	8.132	16.434	

A^1_B	Top Zigzag Edge	8.336	8.036	16.372	0.158
	Bottom Zigzag Edge	8.227	8.303	16.530	
A^2_B	Top Zigzag Edge	8.497	8.461	16.958	2.862
	Bottom Zigzag Edge	7.040	7.056	14.096	
A^3_B	Top Zigzag Edge	6.965	7.004	13.969	-3.162
	Bottom Zigzag Edge	8.580	8.551	17.131	

As we can see from the table 4.2, the charge densities of up spin and down spin in the top and bottom zigzag edges of the reference device are equal and hence there is no significant charge difference among the edges. This supports the degeneracy of the up and down spin states as observed in the density of states spectrum of the reference device depicted in the figures 4.1 (a) and (b). For the other devices, relative to the reference device, we can see a significant charge difference among the top and bottom edges in the charge densities of the up spin as well as down spin states and more generally in the total charge densities of the up and bottom zigzag edges. This charge difference is surely the result of the dopant (boron) effect. Hence, in summation we have found that the origin of as observed spintronicities among the B doped devices are due to the zigzag edge induced effects.

Furthermore we have also investigated the majority local spin density in the central region. As shown in the table 4.3, charge density comparison is performed among the top and bottom halves of the central region.

Table 4.3. Comparison of Charge Densities among the Top and Bottom Halves of the Central Region

Device	Edges	q↑	q↓	q↑ – q↓	Net charge
A^1_B	Top half	9.093	8.893	0.2	0.55952
	Bottom half	11.224	10.865	0.359	
A^2_B	Top half	9.010	9.006	0.004	0.01936
	Bottom half	8.290	8.276	0.014	
A^3_B	Top half	9.077	9.066	0.011	-0.01315
	Bottom half	8.107	8.130	-0.023	

Finally, we can summarize our key findings as follows for B doped devices.

- If **q↑ – q↓** is negative, down spin is dominant in either top or bottom halves of the devices.
- If **q↑ – q↓** positive, up spin is dominant in either top or bottom halves of the devices.
- If the net charge, (q↑ – q↓) top + (q↑ – q↓) bottom**,** is negative, the down spin is dominant in the overall central region of the device and the reverse is true for up spin.

Above these, important conclusions are also corroborated from the table 4.3. Because, the difference in the up and down spin charge densities is positive indicating that up spin

states are the dominant spin states in devices A^1_B and A^2_B. On the other hand, in device A^3_B, since the difference in the up and down spin charge densities is negative, down spin states are the dominant spin states. Hence, it is clear that the above results also comply with the trends that we have obtained in the DOS spectra shown in figure 4.2 for all boron doped devices.

4.4 The Density of States (DOS) spectra for Boron – Nitrogen Doped Ribbons (A_{BN})

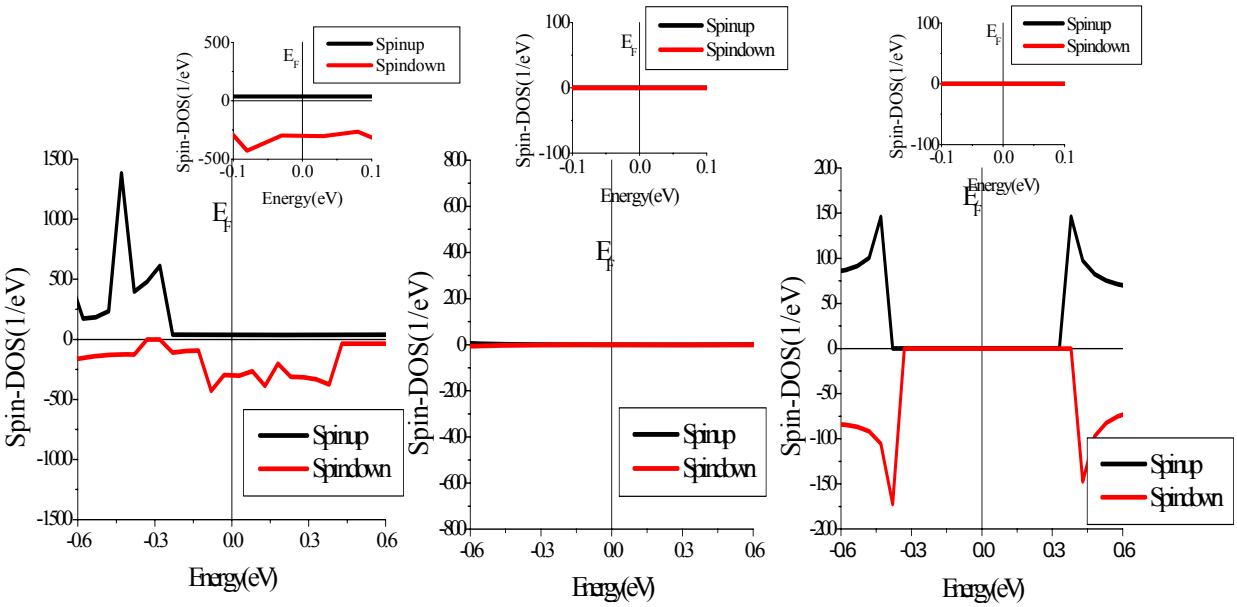

Figure 4.3 Density of States (DOS) spectra for devices a) A^1_{BN}, b) A^2_{BN} and c) A^3_{BN}. The respective inset figures depict the spin for the Dirac fermions at very low energies.

It can be easily noticed from the DOS spectra as depicted in the figure 4.3 that the B – N pair doping at different sites of the edges obliges the ribbon to attain vivid conductivity

states and types in addition to inducing the magnetism. When the B – N pair doping is at the bottom and top terminating hydrogen sites, i.e., device A^1_{BN}, the device attains nearly half metallic state with calculated polarization (P) at E_F of 0.783. If we observe the DOS spectrum for this particular device shown in figure 4.3(a), we can see that the spin down states are the majority spin states near the Fermi level. This can be clearly seen in the zoomed curve of figure 4.3a within the energy range -0.1eV to 0.1eV.

As it is observed in the DOS spectrum of device A^1_B shown in the figure4.2(a) the boron edge decoration (edge doping) at the bottom hydrogen site introduces hole to the edge and shifts the Fermi level to the valence band of the spin states as a result holes are now become the majority up spin carriers. However, when we doped Nitrogen atom which is more electronegative in nature at the corresponding site mentioned in the boron doped ribbon, it is found that the Fermi level shifts to the conduction band of the up and down spin states by setting electrons as up or down spin carriers whichever is in the majority state. A similar situation happened in the device A^1_{BN}, where we have introduced a B – N pair decoration at the opposite hydrogen sites as shown in the figure 4.3(a). This can be ascribed to the higher electronegetivity of Nitrogen atom and the Fermi level shifts to the right. And hence, the DOS of device A^1_{BN} shows that electrons are now the majority down spin carriers.

When the B – N pair doping is done at the bottom and top zigzag edges of different sublattices, i.e., devices A^2_{BN} and A^3_{BN}, the respective devices attained semiconducting state which is shown in their respective DOS spectrum of figures 4.3(b) and (c) respectively. In such sites, instead of magnetism, the dopants affect the conductivity

property of the ribbons. It means that the B – N pair doping at those particular sites opens the band gap of the respective devices. The inset of these also show almost zero contributing states for both spin up and spin down carriers for the low energy electrons, hence presence of negligible states indicates towards the semiconducting properties of the devices

To see the spintronics effect induced to the devices due to the presence of those dopants, we calculated the polarization of the devices at the Fermi level and summarized the results in the following table.

Table 4.4. Calculated polarization at E_F for devices A^1_{BN}, A^2_{BN} and A^3_{BN}

Devices	**Up spin DOS ($D^{\uparrow}$)**	**Down spin DOS ($D^{\downarrow}$)**	**Polarization (P)**
A^1_{BN}	36	300	0.783

As can be seen in table 4.4 above, device A^1_{BN} is a good spin injecting device since we have 300 – 36 = 264 low energy up spin states.

Furthermore, the effect of B-N pair edge decoration (edge doping) on the ribbon is analyzed by calculating the total charge densities of the top and bottom halves of the ribbons. In addition, the dominancy of up and down spin states between top and bottom halves of the devices is investigated calculating the spin charge density differences.

Table 4.5. Total Charge Densities of Top and Bottom Halves of Devices A^1_{BN}, A^2_{BN} and A^3_{BN} and Comparison of Spin State Dominancy

Device	Edges	q↑	q↓	q↑ + q↓	q↑ − q↓
A^1_{BN}	Top half	13.656	12.402	26.062	1.254
	Bottom half	11.518	10.550	10.068	0.968
A^2_{BN}	Top half	9.884	9.895	19.779	-0.011
	Bottom half	8.150	8.162	16.312	-0.012
A^3_{BN}	Top half	10.099	10.112	20.211	-0.013
	Bottom half	7.944	7.956	15.9	-0.012

As we can see in table 4.5 above, the top half for the three devices is superior in the total charge density. This is because the top half of the ribbons is the site in which Nitrogen atom is doped while the bottom half is for boron doping. Nitrogen introduces electrons to the top half and Boron introduces holes to the bottom half. Hence, there are more electrons in the central region of the devices than holes. This fact is clearly seen in the charge density difference of device A^1_{BN} (Table4.5). As we have seen in the DOS spectrum of device A^1_{BN} shown in the figure 4.3(a) electrons are the majority down spin carriers. Therefore, for device A^1_{BN} down spin states are the dominant spin states.

In devices A^2_{BN} and A^3_{BN}, however, up and down spin charge densities in top or bottom half are almost equal and they cancel each other producing no significant charge carriers in the central region of the devices such that the devices become insulators.

4.2 The Density of States (DOS) spectra for Boron - Oxygen Doped Ribbons (A_{BO})

This is our third architecture for spintronic devices. In B – O pair doping, we only replaced Nitrogen with Oxygen with out changing the doping sites. Therefore a similar set analysis like that of the Boron – Nitrogen pair doping can be presented for this devices.

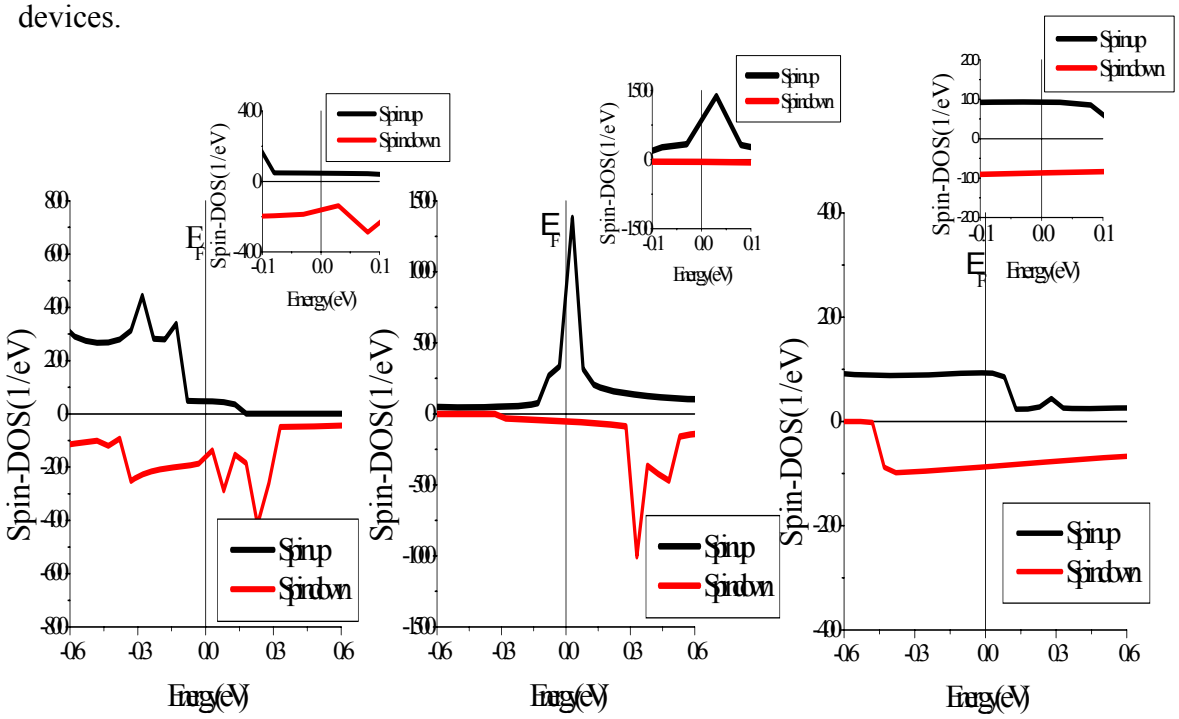

Figure 4.4 Density of States (DOS) spectra for devices a) A^1_{BO}, b) A^2_{BO} and c) A^3_{BO}. The respective inset figures depict the spin for the Dirac fermions at very low energies.

We have noticed from the DOS spectrum of the device A^1_{BO} shown in the figure 4.4(a), the spin is polarized only for the low energy states i.e. states near the Fermi level of energy that ranges from -0.1eV to 0.1eV and the down spin states are the majority spin

states as depicted in the inset of the figure. The calculated polarization (P) at the Fermi level is 0.547, which shows that the device has attained a ferromagnetic state. This can be ascribed to the fact that the majority spin down states are more populated to the right of the Fermi level and electrons are supposed to be the down spin carriers.

Similarly, in the DOS spectrum of the device A^2_{BO} of figure 4.4(a), one can clearly see that spin is polarized in the low energy states. But in this case the up spin states are the majority low energy spin states. They are more populated to the right of the Fermi level indicating that electrons are the spin up carriers. The calculated polarization at the Fermi energy is found to be maximum which is equal to 0.8862. Hence, the device attained nearly half metallic state. However, as the DOS spectrum of device A^3_{BO} shown in the figure 4.4(c) shows there is insignificant difference in the population of low energy states especially with in the energy range of -0.1eV to 0.1eV as also depicted from its inset figure. The calculated polarization at the Fermi energy for this device which is equal to 0.032 is found to be the least among the three B – O doped devices. Hence, the device undoubtedly attained a paramagnetic state.

The calculated polarization values for the three B – O doped devices are summarized in the table below.

Table 4.6. Calculated polarization at E_F for devices A^1_{BO}, A^2_{BO} and A^3_{BO}

Devices	**Up spin DOS ($D^{\uparrow}$)**	**Down spin DOS ($D^{\downarrow}$)**	**Polarization (P)**
A^1_{BO}	47	162	0.550
A^2_{BO}	858	52	0.886
A^3_{BO}	93	87	0.033

Based on the above polarization table (Table 4.6), one can deduce that devices A^2_{BO} and A^1_{BO} are the best spintronic devices. Using device A^2_{BO} one can inject 858 – 52 = 806 low energy up spin states while using device A^1_{BO} one can inject 162 - 47 = 115 low energy down spin states. However using device A^3_{BO} one can inject 93 – 87 = 4 low energy up spin states which is a relatively insignificant number for its spintronc applicability.

To support the results we have obtained from the DOS spectra of the three devices, we have further investigated the total charge densities and up spin and down spin charge density differences in their respective top and bottom halves of the central region. The table 4.7 below summarizes the said data.

Table 4.7. Total Charge Densities of Top and Bottom Halves of Devices A^1_{BO}, A^2_{BO} and A^3_{BO} and Comparison of Spin State Dominancy

Device	Edges	q↑	q↓	q↑ + q↓	q↑ − q↓
A^1_{BO}	Top half	14.040	14.014	28.054	0.026
	Bottom half	11.492	10.602	22.094	0.89
A^2_{BO}	Top half	11.062	10.492	21.554	0.57
	Bottom half	8.249	8.051	16.3	0.198
A^3_{BO}	Top half	11.019	11.191	22.21	-0.172
	Bottom half	8.129	8.138	16.267	-0.009

From table 4.7 above one can observe that the doped top half of the zigzag edge is superior in total charge density among all the three B - O doped devices which clearly shows that there is a significant spin moment (or potential) difference between the edges due to the presence of high electronegative Oxygen atom on one edge and the electropositive Boron atom on the other. This potential difference enables our devices A^2_{BO} and A^1_{BO} to gain highly polarized spintronicity. However, in device A^3_{BO} if we observe up and down spin charge densities in either of top or bottom half of the device we can see an insignificant difference in between them indicating that up and down spin states cancel each other producing little polarization in the central region of the device. At the same time all these results are also corroborated from the DOS spectra of the three B – O doped devices depicted in the figure 4.4.

To sum up, we have investigated half metallicity by doping fully hydrogen saturated 2ZGNR. Polarization results have shown that the full half metallicity is not achieved in our present set of studies. Nevertheless, a nearly half metallic devices have been found which have the potential for spintronics applications. Hence, at the best we can term these doped grpahene ribbon material as good ferromagnetic materials with minimum charge scattering. The table below summarizes the calculated polarization at E_F and total minimum energies of these devices.

Table 4.8. Calculated Polarizations and Total Minimum Energies of the Ferromagnetic Devices

Device	Polarization at E_F (%)	Total Minimum Energy (eV)
A^1_B	96.18	-1850.31
A^3_B	15.6	-1486.45
A^1_{BN}	78.33	-2446.44
A^1_{BO}	54.75	-2829.77
A^2_{BO}	88.62	-2165.19

Based on Table 4.8 above among the doped devices A^1_B, A^1_{BN}, A^2_{BO} are nearly half metallic conformations. Out of the three devices A^1_B holds the highest spin polarization. However in terms of stability A^1_{BN}, which is the least polarized device out of the three nearly half metallic devices is the most stable. Stability of the devices can be described by their total minimum energies. The bigger the negative number, the lesser is the total minimum energy and hence more stable the device will be.

4.6 Investigation of Spintronicity by Creating Vacancies (B-type device)

Vacancies induce impurity states around the Fermi level. When these defects are produced in the same sublattice, the magnetic moments from the defective states can make a ferromagnetic (FM) coupling. The magnetic properties of graphene

nanostructures are intimately related to the sublattice imbalance N_A - N_B in agreement with Lieb's theorem. According to Leib's Theorem, the local magnetic moment can be calculated by using the relation, S = ½ (N_A - N_B); where, S is local magnetic moment, N_A is the number of vacancies created on sublattice A and N_B is the number of vacancies created on sublattice B [26].

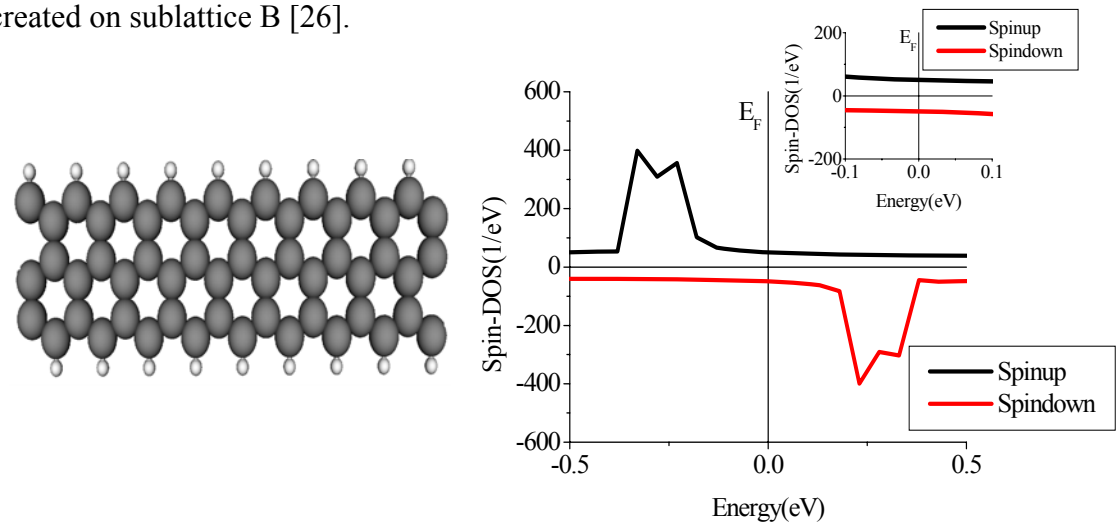

a) *b)*

Figure 4.5 Schematic diagram of a) reference sample 3ZGNR (device B) with width (n) of 3 zigzag rows and b) its corresponding density of states (DOS) spectrum. The respective inset figure shows the low energy spin states.

As we can see from the DOS spectrum of figure 4.5(b), spin up states and spin down states are almost degenerate around the Fermi level which means that there is a balanced (or equal) distribution of the low energy states. This implies that the net magnetic moment in the device is zero and there is no spin polarized transport. This result is expected as far as the ribbon is free from sublattice imbalance as well as the dangling states which could induce magnetism to the ribbon. Therefore to generate a spin polarized transport in the device we have to create unequal distribution of low energy up and down

spin states. To do this we have created a maximum of two vacancies and investigated the changes on the density of states (DOS) spectrum.

The figure 4.6 below shows the device with one vacant atom and its corresponding density of sates (DOS) spectrum.

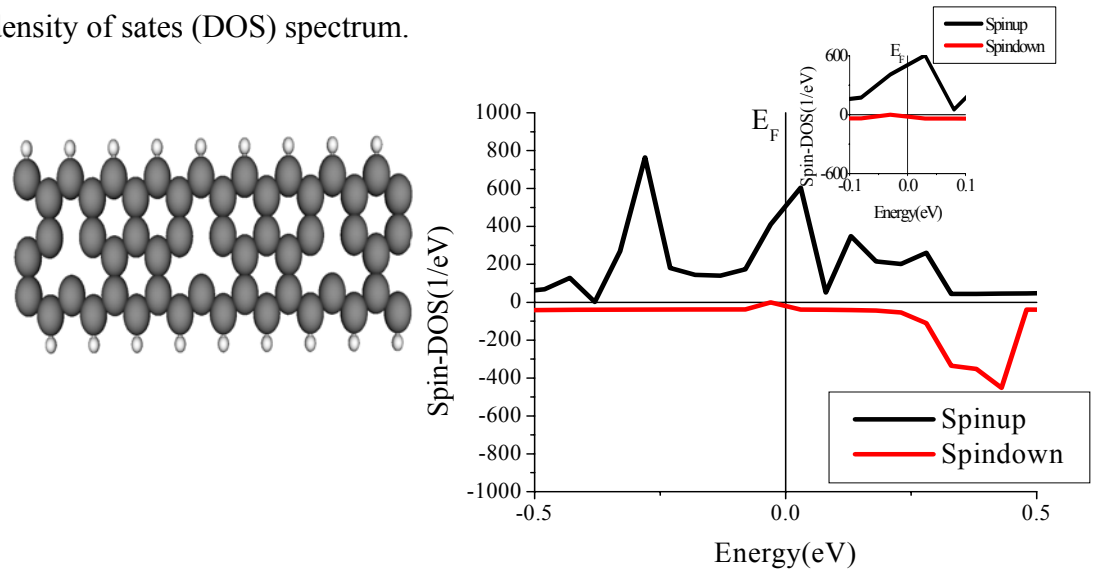

a) B^1_V ***b) DOS***

Figure 4.6 Schematic diagram of a) device B^1_V b) its corresponding density of states (DOS) spectrum [the calculated polarization at E_f = 0.93].

As can be seen in the DOS spectrum shown in the figure 4.6(b), we created unequal distribution in the low energy states which can break spin degeneracy. Within the energy range of -0.1eV to 0.1eV, the corresponding spin up population amounts to an average of 516 states/eV. On the contrary, the corresponding spin down population within the same energy range amounts to an average of 20states/eV. If we calculate the difference in the spin state within the said energy range, we will have 496states/eV of the up spin population near the Fermi level. Thus, we can deduce that spin is now polarized with dominant up spin states. Hence, polarization (P) of 93% is obtained for the device with

one vacancy which is greater than even some of the doped devices. Furthermore, as our polarization calculation showed device B^1_V (the ribbon with one vacancy) has attained a nearly half metallic state.

Our next observation has been made on the device with two vacant atoms (two vacancies)

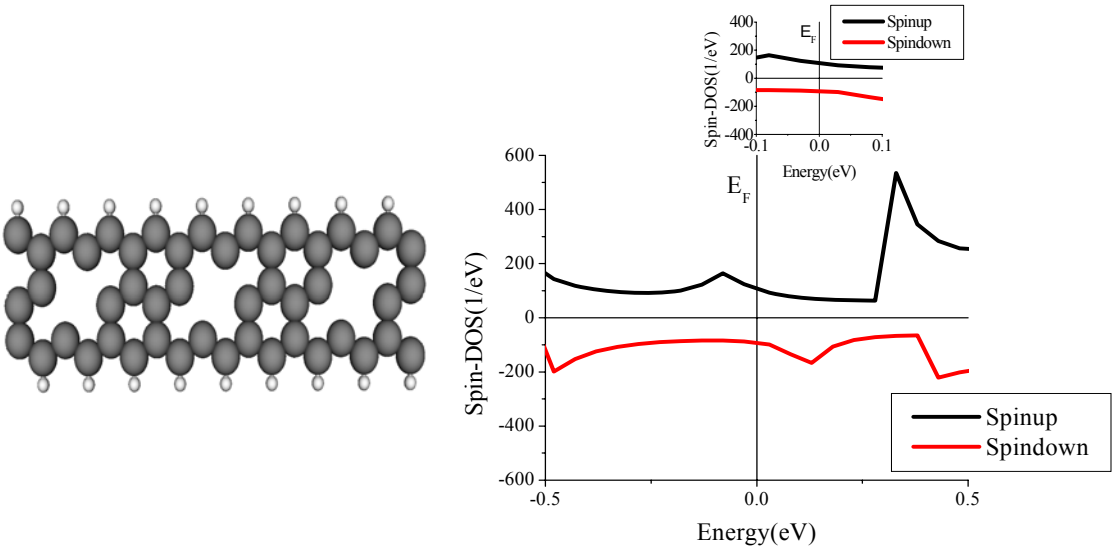

a) B^2_V *b) DOS B^2_V*

Figure 4.7 Schematic diagram of a) device B^2_V and b) its corresponding density of states (DOS) spectrum [the calculated polarization at E_f = 0.076]. The respective inset figure shows the low energy spin states.

From the inset DOS curve of figure 4.7(b), it is observed that the spin up and spin down states occupy same area around the Fermi level indicating that the device has become nearly paramagnetic. Besides, the calculated polarization at the Fermi energy, p = 0.0762, complies with this discussion. Furthermore, from Lieb's theorem, as far as the vacancies are created on different sublattices shown in the figures 4.3(b) & 4.7(a)), magnetic moments are antiferromagnetically coupled, and hence the local magnetic moment is calculated to be zero.

In general, based on the spin polarization results we calculated at the Fermi level for the devices prepared with vacancies, out of the two, the one with a single vacancy has gained better spintronicity than the one with two vacancies.

4.7 Exemplary Applications of as prepared Spintronics Devices in the Magnetoresistive Diodes

Based on the polarization results we got from our ferromagnetic or nearly half metallic devices, the magnetoresistance value for the four nearly half metallic devices could be calculated. Theoretically, it has been proved that the magnetoresistance (MR) value for half metals is infinite which is ideal for spintronic application since they show 100% spin polarization at E_f and thus give lesser spin related power losses. As our calculations showed that huge MR value is obtained from A^1_B, A^1_{BN}, A^2_{BO} and B^1_V which makes them ideal for spintronic applications (Table 4.9).

Table 4.9. Calculated Magnetoresistance (MR) Value for the Nearly Half-Metallic Devices Found

Sample Devices	Polarization (P)	Calculated MR (Ω)
A^1_B	96.18	2468.775
A^1_{BN}	78.33	317.5433
A^2_{BO}	88.62	731.7513
B^1_V	0.93	1280.38

CHAPTER FIVE

5. Conclusions

We have investigated a range of in nano conformations either by dopants or vacancies for half metallic devices. We have used fully hydrogen saturated 2ZGNR and 3ZGNR for the purpose of spin device fabrication. We performed geometry optimization for the modeling of fully relaxed doped devices using Newtonian type structure relaxation algorithm with a force tolerance value of 0.55eV/Å. We have investigated the B, B - N and B - O doping effects on the either sides of the zigzag edges as well as the effect of creating vacancy on the electronic structure of ZGNRs using first principles calculations. It is found that doping B or N or O atoms affects the localized edge states on the two sides differently, which significantly changes the spintrinic property of the ZGNRs. Our calculations suggest that, by jointly applying electron donating atoms such as Nitrogen or Oxygen doping and hole generating or electron accepting atoms such as Born doping at the top and bottom edges of the ribbon, we can directly control the electron occupation of specific edge states as well as enlarge the chemical potential difference between the edges so that nearly half-metallic devices could be produced. This fact provides a new scheme for inducing half-metallicity in ZGNRs and opens up new possibilities for applications of ZGNRs in the field of spintronics.

Furthermore, we have also found that by creating vacancy on different sub lattices of the nZGNR there is a possibility to induce half-metallicity among ZGNRs. Especially we have found un conventionally high FM coupling in single vacancy site samples in

comparison to AFM nature of the double vacancy sites. Lastly, we have demonstrated the exemplary magnetoresistance cmparison among these devices and all four classes of spintronic devices are found suitable for their industrial applications.

References

1. Fujita M, Wakabayasi K, Nakada K and Kusakabe K, J Phys Soc Jap 65 (1996) 1920.
2. Son Y, Cohen M & Louie S, Nature 444 (2006) 347.
3. Kan E J, Li Z, Yang JL and Hou JG, App Phys Lett 91 (2007) 243116.
4. Neto AHC, Guinea F and Peres NMR, Phys World 19 (2006) 36.
5. Novoselov KS, Geim AK, Morozov SV, Jiang D, Zhang Y, Dubonos SV, Grigorieva IV and Firsov AA, Sc Mag 306 (2004) 666.
6. Molitor F, Guttinger J, Stampfer C, Droscher S, Jacobson A, Ihn T and Ensslin K, J Phys 23 (2011) 243201.
7. Neto AHC, Guinea F, Peres NMR, Novoselov KS and Geim AK, Rev Mod Phys 81 (2009) 109.
8. Wu F, Kan E, Xiang H, Wei S, Whangbo M & Yang J, App Phys Lett 94 (2009) 223105.
9. Sergey M, Physics and Applications of Graphene – Experiments, InTech Open (2011) ISBN: 9789533072173, URL: http://www.intechopen.com, Retrieved on 21st March 2012.
10. Son Y, Cohen M and Louie S, Phy Rev Lett 97 (2006) 216803.
11. Shaughnessy M, Ryan S, Damewood L and Fong CY, J Nanomat 2011 (2011) 140805.
12. Kan E, Wu X, Li Z, Zeng X, Yang J & Hou J, J Chem Phys 129 (2008) 084712.
13. Dutta S Manna A and Pati S, Phys Rev Lett 102 (2009) 096601.

14. Zheng XH, Wang XL, Abtew TA and Zeng Z, J Phys Chem (C) 114 (2010) (4193).
15. Groot RA, Mueller FM, Engen PG and Buschow KH, Phys Rev Lett 50 (1983) 2024.
16. Hod O, Barone V, Peralta J and Scuseria G, Nan Lett 7 (2007) 2295.
17. Wolf SA, Chtchelkanova AY and Treger DM, IBM J R and D 50 (2006) 101.
18. Igor Z, Jaroslav F and Das SS, Rev Mod Phys 76 (2004) 324.
19. Slonczewski JC, Phys Rev B 39 (1989) 6995.
20. Meriam W, Collegiate Dictionary, 11th edition, Encyclopedia Britanica (2003).
21. Hohenberg P and Kohn W, Phys Rev 136 (1964) 864.
22. KohnW and Sham LJ, Phys Rev 140 (1965) 1133.
23. Barth U and Hedin L, J Phys (C) 5 (1972) 1629.
24. Ceperley DM and Alder BJ, Phys Rev Lett 45 (1980) 566.
25. ATK: Manual, URL: http://www.quantumwise.com, Retrieved on 21st March 2012.
26. Fernandez Rosssier J and Palacios JJ, Phys Rev Lett 99 (2007) 177204.